J Solid State Electrochem (2006) 10: 329–336
DOI 10.1007/s10008-005-0090-y

ORIGINAL PAPER

A. G. Muñoz · G. Staikov

Electrodeposition of metals on anodized thin Nb films

Received: 26 October 2005 / Revised: 28 November 2005 / Accepted: 6 December 2005 / Published online: 21 February 2006
© Springer-Verlag 2006

Abstract The influence of the electronic properties of oxidized Nb surfaces on the electrodeposition of metals (Me=Co, Cu, Ag) with different equilibrium potentials $U_{\mathrm{Me/Me}^{z}}$ is studied by conventional electrochemical techniques and atomic force microscopy. The results show that relatively thin anodic Nb_2O_5 films (thickness <11 nm) present a frequency-dependent n-type semiconductor behavior, which can be described by the theory of amorphous semiconductor. The Schottky barrier, formed at the a-Nb_2O_5/electrolyte interface, affects the deposition rate of metals with equilibrium potentials more positive than the flat band potential $\left(U_{\mathrm{Me/Me}^{z+}} > U_{\mathrm{FB}}\right)$. Then, the dependence of density of states on the oxide thickness and anodization conditions leads to different extents of the band bending, affecting directly the rate of electron transfer.

Keywords Nb oxide · Electrodeposition · n-Semiconductors

Introduction

The electroplating of metallic layers on semiconductor oxides is a topic of considerable interest in the electronic industry because of its application in the construction of Schottky barriers [1, 2]. This type of structures can be commonly achieved by vapor phase or electrochemical deposition on the thermally generated oxide. However, the first method becomes difficult when the assessment of integrated circuit devices of smaller dimensions is required, mainly due to the size limitation of masks. Anodization and electrochemical deposition offer an excellent alternative to this issue because it allows obtaining thin and good-quality metal and oxide films at low temperatures and costs. In the last years, atomic force microscopy (AFM) has been successfully applied to perform localized anodic oxidation of valve metals to construct lateral metal/oxide/metal nanostructures [3, 4]. In this sense, it is necessary to have better knowledge of the electrodeposition mechanisms on oxidized surfaces to find optimal conditions and explore new construction possibilities. The generation of thin metal films and metal nanoparticles on oxide-covered surfaces has also received great attention in the research and development of nanomagnets as memory units [5] and in the solar cell and sensor technology [6, 7]. However, in spite of the better performance of the electrochemical deposition for the generation and size control of nanoparticles, it was not sufficiently explored for these purposes.

In this paper, we analyze to some extent the mechanisms of electrodeposition of various metals of technological interest on oxidized thin Nb films. As depositing metals, Co, Cu, and Ag were selected to cover a relatively wide spectrum of deposition potentials and to analyze aspects concerning the electronic properties of anodic oxide films. A better comprehension of the basic processes occurring in the metal/oxide/electrolyte interface promises to be very helpful for the development of electronic devices based on metal/oxide/metal structures.

Experimental details

The working electrode was composed of a small piece of silicon wafer covered with 500 nm SiO_2, whereon a 100-nm Nb film was deposited by means of DC-sputter at 10^2 Pa. The samples were used as received, with the presence of a

A. G. Muñoz (✉) · G. Staikov
Institute of Thin Films and Interfaces (ISG-3), and CNI-Centre of Nanoelectronic Systems for Information Technology, Research Centre Jülich, 52425 Jülich, Germany
e-mail: munoz@ww4.ww.uni-erlangen.de
Tel.: +49-9131-8527587
Fax: +49-9131-8527582

Present Address:
A. G. Muñoz
Department of Materials Science, Institute for Surface Science and Corrosion (LKO), University of Erlangen-Nürnberg, Martenstrasse 7, 91058 Erlangen, Germany

native Nb oxide, and were placed into a Teflon holder defining an exposed area of 0.125 cm^2.

Experiments were performed at room temperature in a conventional glass electrochemical cell under N_2-saturated atmosphere using a Pt wire and the system $Hg/Hg_2SO_4/K_2SO_{4(sat)}$ (sse, U^0=0.64 V vs nhe) as counter and reference electrode, respectively. All electrode potentials in the text are referred to this electrode. Electrodeposition was performed from a 0.5 M Na_2SO_4 + 0.5 M H_3BO_3 solution of pH 4.5 containing 0.01 M metal ions Me^{z+}(Me^{z+}=Co^{2+}, Cu^{2+}, Ag^{+}). The addition of boric acid provides a buffering effect during hydrogen evolution. Electrochemical measurements were carried out with a universal electrochemical interface and an impedance spectrum analyzer Zahner IM5d.

The morphology of metal deposits was analyzed by means of ex situ AFM, with a molecular imaging microscope coupled to a nanoscope E controller. Cantilevers with a force constant of 0.10 N m^{-1} and Si uncovered tips (10 nm of curvature radius) were used.

Results and discussion

Anodic oxidation of sputtered Nb films

A detailed characterization of anodically generated Nb oxide films is the necessary first step to get a better understanding of the mechanisms of metal deposition on them. Figure 1 shows a typical cyclic voltammogram for the potentiodynamic anodic oxidation of a sputtered Nb film together with the evolved anodic charge. The appearance of an initial anodic peak is related to the accumulation of charges injected at the interfaces, as already discussed in detail by Lohrengel (cf. [8] and references given therein). On the other hand, the setting of a constant current density at higher anodic potentials indicates that in the deposition solution the oxide growth follows a high field mechanism, in agreement with results reported by others [4, 8–10]. However, the onset of oxygen evolution at U>1.5 V leads to a slight current increase that is also reflected in a slope change in the q vs U plot. Then, a rough estimation of the oxide thickness d_{ox}=12 nm could be made by extrapolation of the first linear part to 4 V and taking an oxide density of 4.4 g cm^{-3}.

To obtain more information about the dielectric properties of the oxide film, the potential dependence of the electrode capacitance C was taken from the imaginary part of the impedance response, assuming as a first approach, that the system behaves as a parallel RC circuit, as is usually made in the study of oxide films. The potential dependence of the inverse of capacitance during the potentiostatic anodic cycle is shown in Fig. 2a. It can be seen that the capacitance shows a constant value in the first 50 mV of the quasistationary forward scan, indicating that the electric field within the native oxide is not large enough for further growth. But this situation is overcome at a potential of about −0.5 V, where the linear increase of the inverse capacitance with the potential arises as a consequence of a continuous oxide growth according to the expression:

$$C^{-1} = \frac{d_{ox}}{\varepsilon\varepsilon_0} = \frac{k\left(U - U^0_{fox}\right)}{\varepsilon\varepsilon_0} \quad (1)$$

where d_{ox} and ε are the thickness and the dielectric constants of the oxide, respectively, k is the oxide formation factor, and U^0_{fox} (=−1.32 V_{sse}) is the standard formation potential of the oxide. Values of k=2.1–2.4 nm V^{-1} and ε =41–46 were reported in the literature for moderate acidic and alkaline electrolytes [4, 8, 10–12]. According to these, thicknesses of 2±0.3 and 12±2 nm for the initial native oxide and the oxide formed after anodization to 4 V, respectively, can be calculated from Eq. (1). Although a direct measurement of the thickness is not possible from our experiments, the values obtained from different data, namely q, C^{-1}, and U, seem to be consistent.

Taking into account that the anodic Nb oxide film behaves as an n-semiconductor, it is expected that a rise of capacitance would occur on approaching to the flat band potential in the reverse potential scan (cf. Fig. 2a). A detailed study of the semiconductor properties of anodically generated Nb oxides was presented by Di Quarto and coworkers in a series of papers [9, 13, 14]. There, the use of the theory of amorphous semiconductor–electrolyte junctions [15–18] for the analysis of semiconductor oxides was emphasized. These authors also advanced toward the calculation of the density of states near the Fermi level by means of impedance measurements in Di Quarto et al. [14].

In an amorphous semiconductor, the net space charge depends on the ionized impurities and the localized states

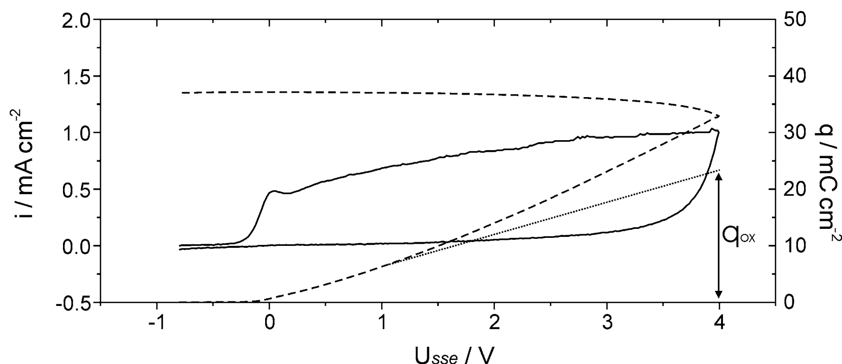

Fig. 1 Anodic oxidation of Nb film 0.5 M Na_2SO_4+0.5 M H_3BO_3 (pH 4.5). v=0.1 V s^{-1}. U_i=−0.8 V

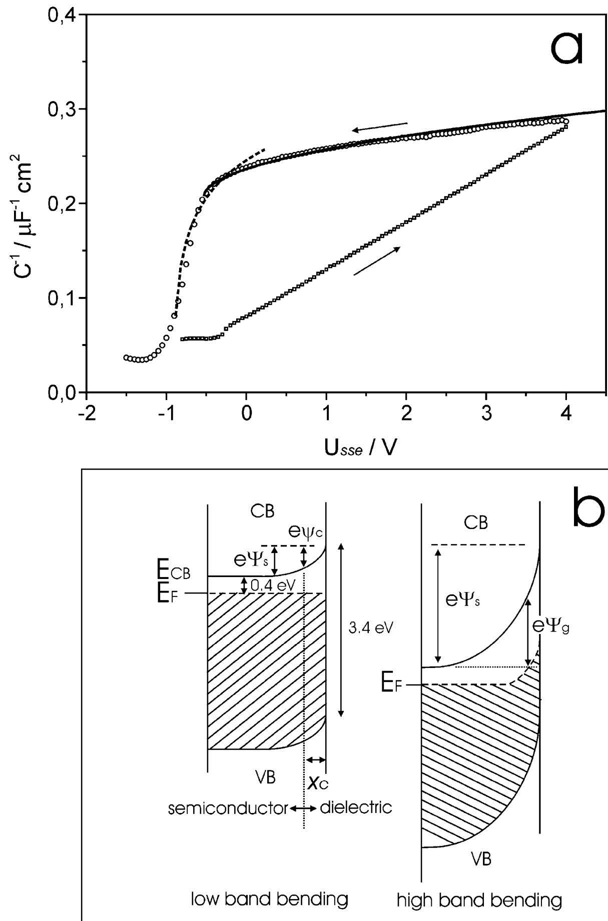

Fig. 2 **a** Potential dependence of the imaginary impedance response expressed as the inverse of capacitance during the quasistationary anodization of Nb film. ΔU=10 mV, f=300 Hz. *Dotted lines* and *full lines* are adjusted curves corresponding to expressions (2) and (3) for low and high band-bending, respectively. **b** Schematic representation of band bending in the reverse potential scan

within the band gap (Fig. 2b). Therefore, the potential distribution and the AC response depend on the distribution of density of states within the gap. This conducts to a frequency dispersion of the capacitance, which in turn makes it inappropriate to use the classical Mott–Schottky expression for estimating the flat band potential and density of donors.

The theory of amorphous semiconductor is based on the exponential correlation between the relaxation time for electron emission of the gap states (τ) and their position with respect to the conduction band, $\tau = \tau_0 \exp[(E_F - E_{CB})/kT]$, E_F being the Fermi energy level. Thus, for a given frequency ω, there will be a point of the Schottky barrier defined by the maximum relaxation time for which the states can still respond (ψ_c). Then, the Schottky barrier can be separated in two zones: $\psi_{(x)}<\psi_c$ where the Fermi level states will not respond (dielectric behavior) and $\psi_{(x)}>\psi_c$ where the response will be essentially complete. In other words, the system behaves as a semiconductor with a band bending ψ_c and a capacity $C(\psi_c)$ in series with an outer dielectric layer, whose capacity is given by $\varepsilon\varepsilon_0/x_c(\psi_s, \omega)$ (see Fig. 2b). It follows that these two zones can be modeled by two capacitors in series for which the total capacitance, for the case of a constant density of states N, is given by [12]:

$$C^{-1}(\omega, \psi_s) = \frac{1}{(\varepsilon\varepsilon_0 e^2 N)^{1/2}}\left[1 + \ln\frac{\psi_s}{\psi_c}\right] \quad (2)$$

where ψ_s is the band bending. This expression gives an adequate description of the potential dependence of capacitance at low band-bending conditions, i.e., if $e\psi_s<[E_g/2 - (E_{CB} - E_F)]$.

For high band-bending conditions, Cohen and Lang [18] demonstrated that the state occupancy can be pinned at the midgap in a near-surface layer if equilibrium conditions for electronic exchanges between the gap states and the valence and conduction bands are admitted (Fig. 2b). Then, under the hypothesis of a constant density of states, the following analytical expression for the total capacitance was derived [15]:

$$C^{-1}(\omega, \psi_s) = \frac{1}{(\varepsilon\varepsilon_0 e^2 N)^{1/2}}\left\{\ln\frac{\psi_g}{\psi_c} + \left[1 + \frac{2(\psi_s - \psi_g)}{\psi_g}\right]^{1/2}\right\} \quad (3)$$

where ψ_g is the potential corresponding to the intersection point of the midgap with the Fermi level. This means that at $\psi>\psi_g$ the electron occupancy remains pinned and no further ionization of gap states occurs with increasing polarization.

A good reproduction of the experimental capacitance data for an oxide grown potentiostatically (cf. the reverse scan in Fig. 2a) is obtained with Eqs. (2) and (3) for low and high band-bending conditions taking values of N=6.5×10^{20} eV^{-1} cm^{-3} and 1.75×10^{21} eV^{-1} cm^{-3}, respectively. These results confirm that the theory of amorphous semiconductors offers a reliable description of the dielectric properties of anodic oxides generated on sputtered Nb films. The fact that different values of the density of states are obtained in the low and high band-bending regions may be ascribed to the generation of different types of mobile defects on increasing the electric field within the oxide film. Nevertheless, we will limit our study to the low band-bending zone due to the fact that metallization is exceptionally carried out at potentials higher than 1 V.

Figure 3 shows the frequency dependence of the capacitance curves for an oxide film formed after potentiodynamic anodization to 4 V. It was found that the curves obtained within a frequency region from 1 kHz to 30 Hz could be well-fitted by Eq. (2). A value of N=4.5±0.3×10^{20} eV^{-1} cm^{-3} and a flat band potential U_{FB}=−0.9±0.08 V could be estimated. The value of the flat band potential is in agreement with that reported by Di Quarto et al. [13] for thin anodic oxides. The fact that ψ_c presents a linear dependence with log ω with a slope of about 60 mV dec^{-1} is in accordance with the theory of amorphous

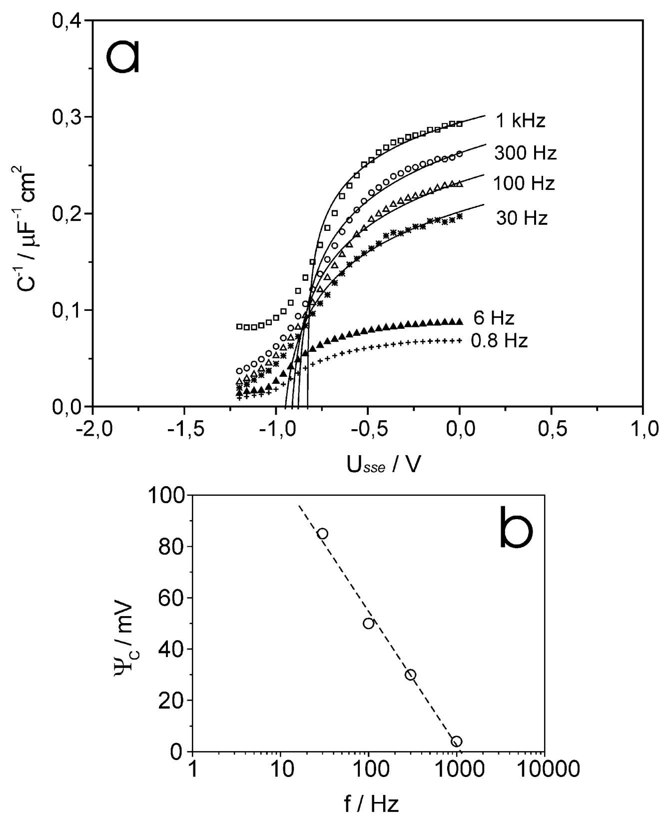

Fig. 3 **a** Potential dependence of the inverse of capacitance obtained at various frequencies on an anodic oxide generated potentiodynamically to 4 V. ΔU=10 mV. *Lines* denote curves obtained by fitting the experimental curve to the expression of low band-bending (2). **b** Frequency dependence of the parameter ψ_c

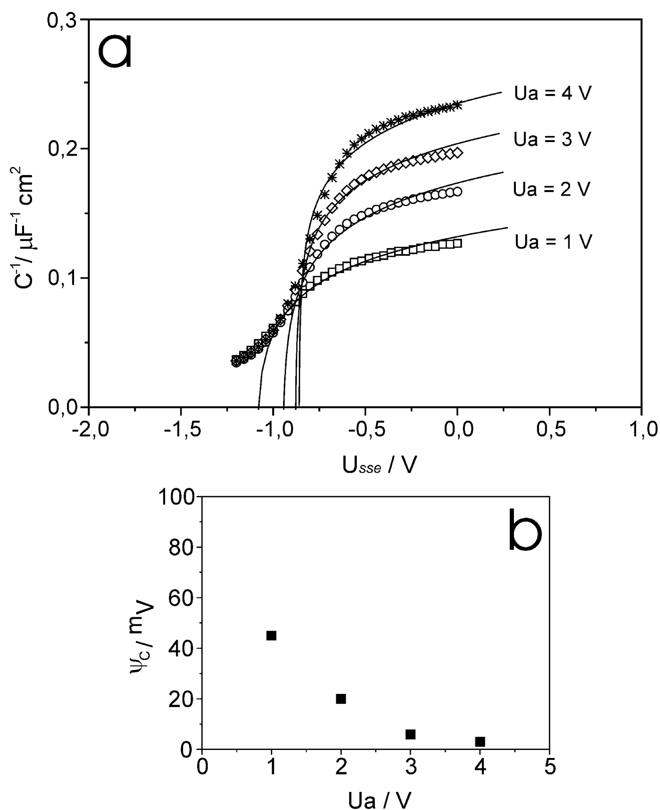

Fig. 4 **a** Potential dependence of the inverse of capacitance obtained at various frequencies on anodic oxides generated potentiodynamically to different successively increasing potentials. ΔU=10 mV, f=300 Hz. *Lines* denote curves obtained by fitting the experimental curve to the expression of low band-bending (2). **b** Dependence of the parameter ψ_c on the anodic limit

semiconductor. At frequencies lower than 30 Hz, however, a marked capacitance increase is observed. This is probably due to the contribution of the surface states to the total capacitance.

A similar analysis performed on oxides formed after successive anodization cycles with an increasing anodic limit reveals the considerable influence of the anodization conditions on the final density of states (cf. Fig. 4). For instance, it can be seen how the potential ψ_c decreases with the anodic limit as a direct consequence of an increment of the space charge fraction with a dielectric behavior. On the other hand, the density of states calculated from the fitting procedure N=15×10^{20} eV^{-1} cm^{-3} suggests a more defective oxide structure if we compare this result with that after anodizing potentiostatically to 4 V. This fact is also reflected in an increase of U_{FB} (obtained by fitting) from −1.1 to −0.86 V on increasing the anodic limit from 1 to 4 V, respectively.

Metal deposition

Deposition of Co

To analyze the influence of the oxide film on the deposition of Co, cyclic voltammetries were performed on Nb covered with native oxide and after the anodization to 4 V (Fig. 5a). In the two cases, the beginning of deposition at U<−1.4 V points out a large nucleation overpotential ($U^0_{sse}= -0.97$ V). The abrupt current increase immediately after the cathodic peak is a direct consequence of the onset of hydrogen evolution on the substrate and on the electrodeposited metal clusters.

It must be noted that in spite of the presence of an oxide film, the deposition does not seem to be affected after anodization. This result contrasts with those presented by other researchers concerning the deposition of Cu on anodized Ta [19], where the exponential decrease of the deposition current was attributed to a resonance type of tunneling process involving the hopping of electrons between states within the oxide gap. In this case, however, the deposition of Co occurs in the accumulation region of Nb oxide, where an increase of the capacity together with a decrease of the charge resistance is expected. Figure 5b shows the potential dependence of the total resistance taken from impedance measurements. It can be observed that it decreases near the flat band potential up to reach the electrolyte resistance toward more cathodic potentials. Therefore, as expected, the substrate behaves like a metal in this potential region.

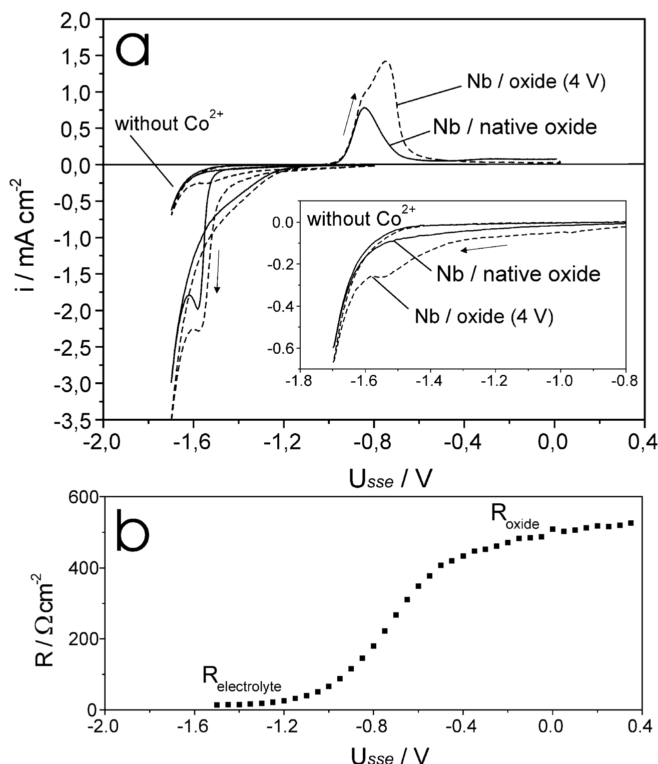

Fig. 5 **a** Potentiodynamic scans performed in 0.5 M Na_2SO_4+0.5 M H_3BO_3 solution with and without 0.01 M Co^{2+} on oxidized Nb surfaces. *Full lines* represent native oxide (d_{ox}~2 nm), while *dotted lines* represent Nb surfaces after potentiodynamic anodization to 4 V (d_{ox}~10 nm). v=0.01 V s^{-1}. *Insert*: scans performed in the absence of Co^{2+}. **b** Parallel resistance for a 4 V oxide obtained at 300 Hz

The presence of a cathodic peak observed at −1.6 V after anodization to 4 V in the solution without Co^{2+} (cf. insert in Fig. 5a) may be related to the incorporation of H^+ into the amorphous oxide [20]. It was reported that the penetration of H into Nb oxide during the cathodic polarization leads to the formation of bronzes of the type $H_xNb_x^{(4+)}Nb_{2-x}^{(5+)}O_5$ [21] together with a substantial modification of the conductivity [21] and the photoelectrochemical response [22, 23]. Then, the effect seems not to be favored in the native oxide, as can be inferred from the absence of a cathodic wave before the onset of hydrogen evolution in the voltammetric response (insert in Fig. 5a).

In spite of similar cathodic voltammetric responses on native and anodic oxides, a higher anodic dissolution charge is observed, however, in the reverse scan on the anodized surface (dotted line in Fig. 5a). This fact could be explained in terms of a higher conductivity of the anodic oxide given by the higher permeability of H^+ into it during the cathodic polarization.

The first stages of Co deposition were analyzed by means of the current–time response after applying potentiostatic pulses of different values on Nb with the presence of a native and an anodic oxide (Fig. 6). In the two cases, the current transients initially present an exponential decrease due to the charging of the capacity of the system oxide/

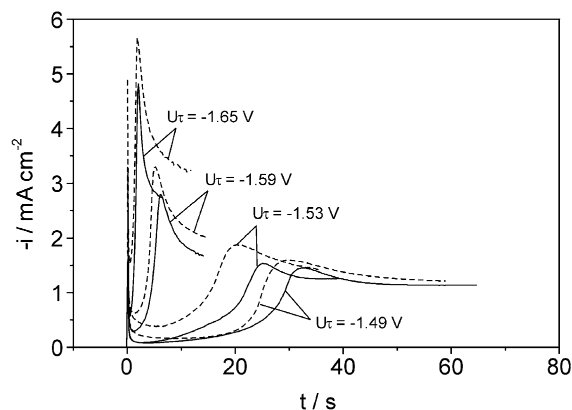

Fig. 6 Current transients obtained after applying different potential steps on Nb film covered with a native oxide (*full lines*) and after potentiodynamic anodization to 4 V (*dotted lines*). Ui=−0.8 V; Solution: 0.5 M Na_2SO_4+0.5 M H_3BO_3+0.01 M Co^{2+}

electrolyte. This process is followed by an induction period of time characterized by a linear current increase, after which a rapid increase to a maximum is observed. In the case of an anodized surface, a shift of the transients to shorter times together with a higher induction current can be observed. These effects, which are in correspondence with the voltammetric results, can be interpreted in terms of the generation of a more defective oxide due to a larger insertion of H during the induction time, which accelerates the nucleation process.

The shape of transients resembles that usually observed in the presence of a kinetically controlled growth of hemispheres, as shown by Abyaneh and Fleischmann [24, 25] for the deposition of Ni. Nevertheless, the complexity of the given analytical expressions and the concomitant hydrogen evolution on the freshly deposited clusters make our analysis difficult. The analysis of the evolution of morphology of the growing clusters helped to obtain some additional information for characterizing the deposition process. The AFM images shown in Fig. 7 reflect the evolution of surface morphology taking place in the rising part of a transient obtained at −1.53 V on Nb covered with native oxide. The image taken at 18 s does not show important morphology differences with the substrate. This suggests that the initial linear current increase would correspond to a side reaction, viz, the hydrogen discharge. On the other hand, the image taken at 25 s indicates that the rapid current increase after 20 s corresponds to the growth and coarsening of very flat metal clusters with average height and width of 30 and 200 nm, respectively. The different sizes of growing clusters suggest that a progressive type of nucleation has taken place. It must be also noted that the current maximum coincides with a complete surface coverage, it being in accordance with the model of kinetically controlled growth of hemispheres. No significant changes of the morphology are observed at longer deposition times. An important feature to be noted is the possibility of obtaining relatively smooth and adherent homogeneous metal layers of Co,

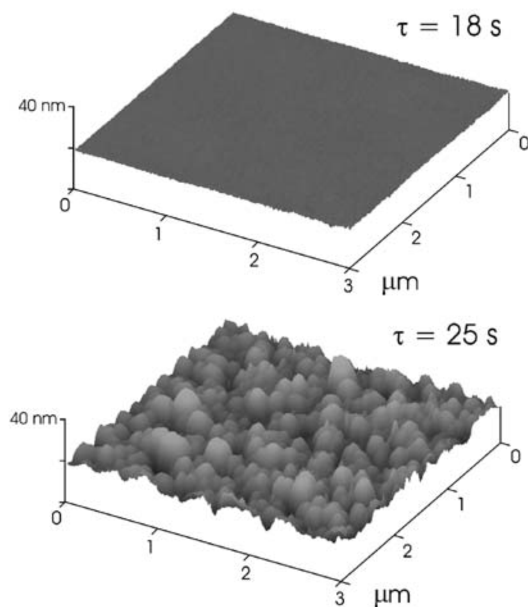

Fig. 7 3 µm×3 µm AFM images showing the morphology of Co deposits generated potentiostatically 0.5 M Na_2SO_4+0.5 M H_3BO_3+ 0.01 M Co^{2+} solution at −1.53 V after different deposition times on Nb film covered with native oxide

which can be also very useful as a seed layer for the deposition of other metals.

Deposition of Cu and Ag

We could observe that in the case of Co deposition, the presence of an oxide film with n-type semiconducting properties does not represent a barrier for the deposition of a metal whose thermodynamic equilibrium potential lies at more negative values than the flat band potential. Therefore, couples such as $Cu/Cu^{2+}\left(U^0_{\rm sse} = -0.418\ {\rm V}\right)$ and $Ag/Ag^{+}\left(U^0_{\rm sse} = 0.041\ {\rm V}\right)$ were investigated.

The cyclic voltammetries performed in Cu^{2+}-containing solutions (Fig. 8a) show that the deposition of Cu occurs at potentials lower than −0.5 V in the presence of a native oxide, showing a lower deposition overpotential than that for Co. Here, however, an increase of the overpotential with increasing anodization limit is observed. This result can be explained if we take into account that the deposition of Cu takes place in the depletion region of the oxide, that is, in the presence of a Schottky barrier. Therefore, the decrease of the density of defects generated when anodization is driven to increasing potentials is reflected in an increasing width of the Schottky barrier. As a consequence, lower rates of electron transfer without modifications of the deposition mechanism are expected. The increase of the Schottky barrier with anodization potential also leads to a marked diode behavior, pointed out by a lower dissolution rate of deposited particles.

The current transients recorded after applying potential pulses of different values on an anodized surface (Fig. 8b) show in all cases the presence of a current maximum fol-

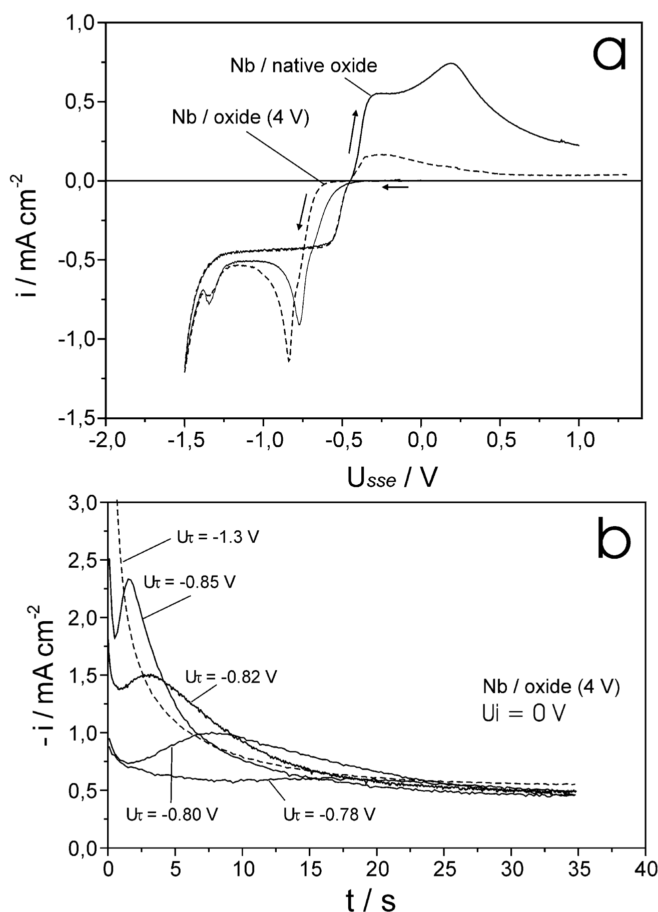

Fig. 8 **a** Cyclic voltammetries performed in 0.5 M Na_2SO_4+0.5 M H_3BO_3+0.01 M Cu^{2+} solution on Nb film covered with a native oxide (*full lines*) and after potentiodynamic anodization to 4 V (*dotted lines*). v=0.01 V s^{-1}. **b** Current transients obtained after applying different potential steps on Nb after potentiodynamic anodization to 4 V. Ui=0 V

lowed by an exponential decay according to the Cottrell's relation $i \propto t^{-1/2}$. This means that the deposition process may be described by the model of diffusion-controlled growth of clusters. An inspection of the AFM images obtained after 35 s of deposition at −0.82 V (Fig. 9) reveals the presence of dispersed flat particles of similar sizes of 100-nm height and 500-nm width in average (cf. Fig. 9a). A very different surface morphology is observed at sufficiently higher overpotentials, where a homogeneous and smooth metal film constituted by particles of 15-nm height and 150-nm width in average is obtained (cf. Fig. 9b). This figure is in agreement with a potential dependent nucleation rate. Thus, the number of metal particles reflects the extent of occupancy of active sites reached before they have been inactivated by depletion effects.

The effects introduced by the presence of a Schottky barrier on the deposition process in the depletion region of the oxide is markedly pointed out by the presence of very different voltammetric responses obtained in Ag^+-containing solutions after increasing the anodization potential (Fig. 10). In effect, the shoulder observed for an oxide

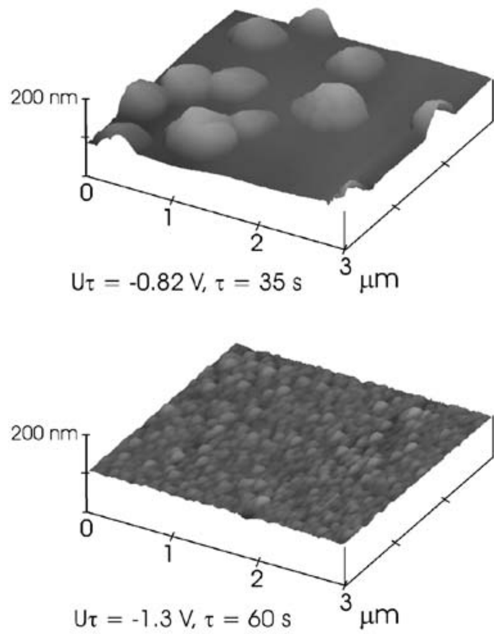

Fig. 9 3 µm×3 µm AFM images showing the morphology of Cu deposits generated potentiostatically at different conditions on Nb film covered with an anodic oxide grown potentiodynamically to 4 V

formed at 0.5 V transforms in a sharp peak if the voltammetry is performed after the anodization to 4 V (U=−0.75 V). Because the equilibrium potential for Ag/Ag^+ is very far from the oxide flat band potential, the charge transfer process is strongly hindered by a deep band bending. Therefore, it is expected that deposition can be only observed after a sufficient decrease of the potential barrier. Then, the flat deposition wave observed between 0 V and −0.5 V after anodizing to 4 V can be attributed to a resonance tunnelling process. In this sense, it is interesting to note that the deposition of Cu and Ag take place at the same potential for a surface anodized to 4 V, giving further support for our hypothesis.

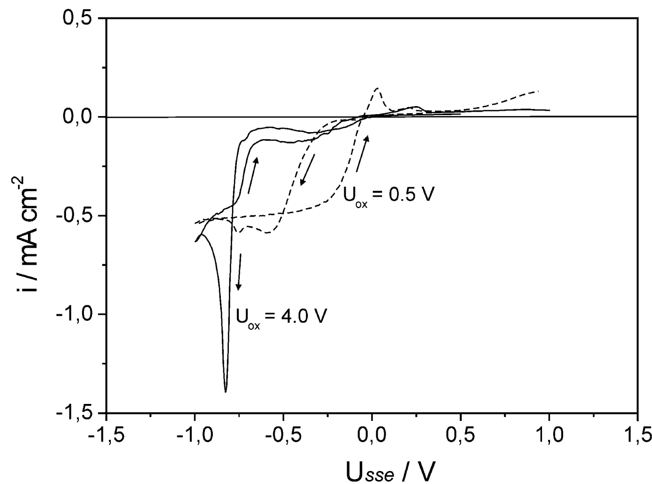

Fig. 10 **a** Cyclovoltammograms performed in 0.5 M Na_2SO_4+0.5 M H_3BO_3+0.01 M Ag^+ solution on Nb film previously anodized to different potentials. v_{ox}=0.1 V s^{-1}, v=0.01 V s^{-1}

Influence of oxide film on deposition

The formation of a Schottky barrier in the depletion zone of the oxide affects the rate of electron transfer at potentials more positive than the flat band condition. Thus, there is a potential threshold for the beginning of metal deposition defined by the barrier height in the electron tunnelling. Radisic et al. [19] found that the density of copper islands decreases exponentially with oxide thickness on anodized Ta. They explained this result in terms of the decreasing effective potential for nucleation due to the potential drop in the oxide. However, the semiconducting properties shown by this oxide at negative potentials were not analyzed. The complete study of the electronic properties carried out by Schultze and Macagno [26, 27] on Ta oxides revealed a change in semiconductor/insulator with increasing oxide thickness. This occurs as a consequence of a linear increase of the thickness of the space charge layer with the oxide thickness. This means, on the other hand, that the density of donors must decrease according to

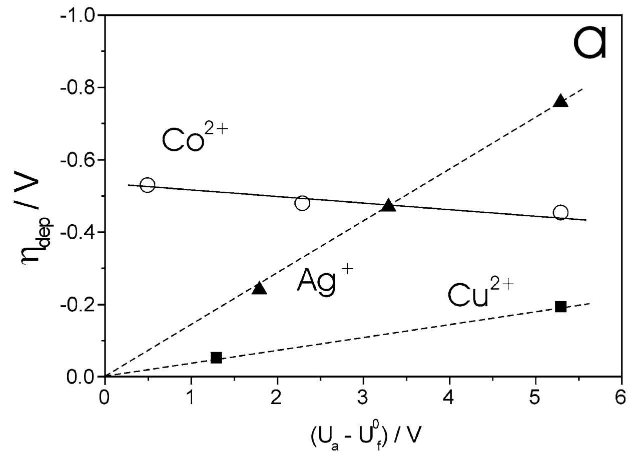

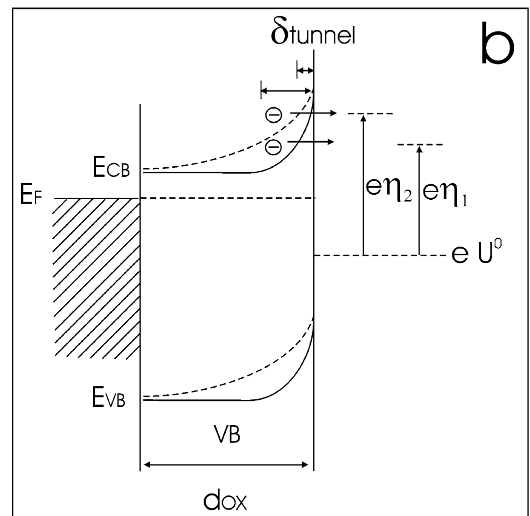

Fig. 11 **a** Deposition potentials for various elements on anodized Nb film as a function of the anodization potential (U_{fox}=−1.29 V). **b** Energy diagram showing the band bending in the oxide at different applied potentials

$N \propto d_{ox}^{-2}$. A similar result was reported by Schulze and Heusler [28] on passive Nb.

Figure 11a shows comparative plots of the threshold overpotentials (η_{dep}) for massive deposition as a function of the anodization potential. This graph highlights how the overpotentials shift toward more negative values for elements whose equilibrium potentials are situated above the flat band potential (U_{FB}~−0.95 V). It must be also noted, that the extrapolation of the linear dependence to the oxide formation potential, U^0_{fox} , for Cu^{2+} and Ag^+ solutions is very close to their equilibrium potentials, indicating low overpotentials for the nucleation. From these results, it is clear that the thickness of the space charge layer play a key role in determining the deposition rate. This is also closely related with the density of states, which decreases with the oxide thickness. These ideas can be better visualized in the scheme presented in Fig. 11b, where it is shown how the large band-bending generated on increasing the potential makes the charge transfer more difficult, as in the case of Ag deposition. The reduction of the density of defects with increasing anodization potential gives rise to an increase of the space charge layer thickness, which in turn conducts to an increase of the tunnelling distance (δ_{tunnel}). Therefore, the applied overpotentials must be increased to obtain the same deposition currents.

Conclusions

The electronic properties of very thin oxide films (<11 nm) generated by anodization of sputtered Nb were analyzed in terms of the theory of amorphous semiconductors. According to this, a concentration of defects N=4–15 eV^{-1} cm^{-3} and a flat band potential U_{FB}=−0.9±0.08 V was determined. The n-semiconducting behavior of the oxide has important consequences for metal deposition at potentials $U > U_{FB}$. Thus, the formation of a Schottky barrier introduces an electronic barrier that affects the deposition rate. Then, the decreasing deposition rate with increasing anodic oxide can be explained in terms of the dependence of the density of states on the oxide thickness and conditions of anodization, which in turn, conducts to different extents of the band bending.

Acknowledgements The authors acknowledge the Institute of Thin Films and Interfaces for the financial support of this work. A.G.M. wishes to acknowledge gratefully the Alexander von Humboldt Foundation for a grant.

References

1. Molina CA, de Oliveira-Versic L, Vazdar M (2004) Mater Lett 58:3518
2. Azizi A, Sahari A, Felloussia ML, Schmerber G, Mény C, Dinia A (2004) Appl Surf Sci 228:320
3. Matsumoto K, Gotoh Y, Maeda T, Dagata JA, Harris J (2000) Appl Phys Lett 76:239
4. Heidelberg A, Rozenkranz C, Schultze JW, Schäpers Th, Staikov G (2005) Surf Sci 597:173
5. López-Díaz L, Klaui M, Rothmann J, Bland JAC (2002) J Magn Magn Mater 242–245:553
6. Yae S, Kitagaki M, Hagihara T, Miyoshi Y, Matsuda H, Parkinson BA, Nakato Y (2001) Electrochim Acta 47:345
7. Täschner C, Pácal F, Leonhardt A, Spatenka P, Bartsch K, Graff A, Kaltofen R (2003) Surf Coat Technol 174:81
8. Lohrengel MM (1993) Mater Sci Eng R11:243
9. Piazza S, Sunseri C, Di Quarto F (1990) J Electroanal Chem 293:69
10. Li Y-M, Young L (2000) J Electrochem Soc 147:1344
11. Schwartz RJ, Chiou YL, Thompson HW (1970) Thin Solid Films 6:81
12. Schultze JW, Lohrengel MM (2000) Electrochim Acta 45:2499
13. Di Quarto F, Piazza S, Sunseri C (1990) Electrochim Acta 35:99
14. Di Quarto F, La Mantia F, Santamaria M (2005) Electrochim Acta 50:5090
15. Da Fonseca C, Ferrera MG, Da Cunha Belo M (1994) Electrochim Acta 39:2197
16. Archivald IW, Abram RA (1983), Phil Mag B 48:111
17. Archivald IW, Abram RA (1986) Phil Mag B 54:421
18. Cohen JD, Lang DV (1982) Phys Rev B 25:5321
19. Radisic A, Oskam G, Searson PC (2004) J Electrochem Soc 151:C369
20. Cabanel R, Chaussy J, Mazuer J, Delabouglise G, Joubert JC, Barral G, Montella C (1990) J Electrochem Soc 137:1444
21. Schwitzgebel G, Unruh T (1995) J Solid State Electrochem 115:260
22. Hayashi Y, Miyakoshi T, Masuda M (1991) J Less Common Met 172:851
23. Hayashi Y, Arita M, Koga K, Masuda M (1995) J Alloys Compd 231:702
24. Abyaneh MY (2002) J Electroanal Chem 530:82
25. Abyaneh MY, Fleischmann M (2002) J Electroanal Chem 530:89
26. Macagno V, Schultze JW (1984) J Electroanal Chem 180:157
27. Schultze JW, Macagno VA (1986) Electrochim Acta 31:355
28. Heusler KE, Schulze M (1975) Electrochim Acta 20:237